=== **SOLIDS AND LIQUIDS** ===

MECHANISMS OF IRON DIFFUSION IN α-Ti

© 2024 N. D. Gorev[a, b], A. V. Bakulin[a*], S. E. Kulkova[a, b]

[a] Institute of Strength Physics and Materials Science, Siberian Branch, Russian Academy of Sciences, 634055, Tomsk, Russia

[b] National Research Tomsk State University 634050, Tomsk, Russia

*e-mail: bakulin@ispms.ru

Abstract. Within the transition state theory and the projector augmented-wave method, the mechanisms of iron diffusion in α-Ti were studied. The formation energies of interstitial and substitution defects, as well as the barriers of iron migration in α-Ti along possible paths through both interstitial and vacancy mechanisms were calculated. It was confirmed that the most preferred position for an iron interstitial atom is a crowdion, which formation energy is only 0.17 eV higher than that of iron defect on titanium site. Analytical expressions for the temperature-dependent diffusion coefficients of iron in two crystallographic directions for the interstitial mechanism were obtained by the Landman method. In general, the coefficients of iron diffusion in α-Ti and its anisotropy are consistent with experimental data, while the corresponding diffusion coefficients for the vacancy mechanism are several orders of magnitude lower. The obtained results allow us to conclude that the anomalously fast diffusion of iron in α-Ti is due to the interstitial mechanism.

1. INTRODUCTION

Titanium and its alloys possess a complex of unique mechanical properties, making them promising materials for application in aerospace, automotive, shipbuilding, and other industries. The development of materials based on them with improved functional characteristics and mechanical properties remains a relevant task for many decades [1]. It is known that technically pure titanium has high corrosion resistance, including in aggressive environments containing chlorine and its derivatives, organic compounds with oxygen, and others. However, the addition of alloying impurities can significantly change its corrosion behavior. Furthermore, one of titanium's advantages is the possibility of its strengthening by oxygen, nitrogen, and small additions of other elements (for example, iron and palladium) to obtain different grades of metal suitable for numerous technological applications. The main difference between titanium grades lies in the content of oxygen and iron. Iron, along with elements such as chromium, manganese, cobalt, nickel, and others, belongs to β-eutectoid elements that stabilize the β-phase, lowering the β−α phase transformation temperature, equal to 1556 K. [2] Unlike β-isomorphous elements (Mo, V, and Ta), the solubility of iron in α-Ti is small, about 0.05 at.% [3]. Impurity diffusion can lead to local changes in their concentration and negatively affect titanium properties.

Many processes in materials and their mechanical properties are related to atomic mobility. Knowledge of diffusion coefficients and anisotropy is very important for understanding deformation processes in alloys, thermal stability of protective coatings, creep resistance, and other characteristics. Information about migration barriers and diffusion mechanisms is necessary for a deeper understanding of oxidation

and hydrogenation processes in materials, as well as the influence of impurities on these processes [6,7]. In this regard, the study of microscopic mechanisms of diffusion of various elements in titanium and its alloys appears important from both theoretical and practical perspectives. Establishing factors affecting the diffusion of impurities that negatively impact material properties allows expanding their application scope.

Despite intensive experimental studies of atomic diffusion in metals and alloys, theoretical calculations of diffusion properties remain rare. In most works, authors calculate migration barriers of impurities between individual interstitial positions, often considering only a limited set of these positions. Conclusions about the preferential diffusion of impurities in certain crystallographic directions are typically made based on the analysis of obtained migration barrier values. At the same time, the fact that atomic diffusion can occur not only along selected directions but also along paths where an atom shifts in both directions simultaneously is not taken into account. Density Functional Theory (DFT) [8] together with transition state theory [9] allows understanding the mechanisms of diffusion and self-diffusion in materials with various crystal structures. With the emergence of algorithms enabling the calculation of barriers along minimum energy paths within several modern software codes, the number of publications on this topic has increased significantly. Most works are devoted to studying the diffusion of light interstitial impurities such as hydrogen or oxygen (see [10−17] and references therein). However, estimating the temperature-dependent diffusion coefficient, even using simplified models, also requires the development of appropriate programs, so such calculations remain rare.

In work [18], self-diffusion of metals with HCP structure (Mg, Zn, Ti, Zr and Hf) was studied. An analysis was carried out on the influence of several factors on migration barrier values: plane wave cutoff energy, k-point grid, supercell size, and structural optimization scheme. It was shown that the supercell size strongly affects migration barriers in d-metals (Ti, Zr and Hf), but they remain practically unchanged in the case of Mg. It was established that the difference in migration barriers in the basal plane and between them decreases with increasing supercell size. The optimization of supercell shape and volume also affects migration barriers more significantly when they are calculated in a small-sized supercell. Overall, the calculated self-diffusion coefficients [18] show good agreement with experiment.

It should be noted that substitutional impurity diffusion has been studied much less by *ab initio* methods than interstitial one. For example, in a recent work [19], diffusion coefficients were calculated for impurities of ten elements (Si, Ti, V, Ta, Ru, Cr, Te, Tc, Ir and Y) in Nb. Migration barriers were obtained for these elements along possible diffusion paths. The results of this work are in good agreement with available experimental and earlier theoretical data for individual impurities. The difference in activation energy from experimental values for several impurities is 0.3−0.6 eV, and a slightly smaller deviation from earlier theoretical results was obtained for Ti and Ru impurities [20].

The dependence of the coefficient on the atomic diffusion mechanism (vacancy or interstitial) was also studied in α-Ti. It is believed that rapid diffusion of Fe, Co, Cr and Ni atoms in α-Ti may be related to the interstitial mechanism [21] and relatively weak atomic bonding between impurity and matrix atoms. The diffusion coefficient of Fe and Co is 7−8 orders of magnitude higher than the self-diffusion coefficient of titanium [22]. In the case of Al, Ga, Ge, Nb, Ta, Si, Sn and other elements, the vacancy mechanism was proposed as dominant [23, 24], with calculated coefficients showing good agreement with experiment. Works [25, 26] showed that for Fe and Co in α-Zr, the formation of an interstitial defect is more favorable than a substitutional defect, while in α-Ti the situation is reversed [25, 26]. Impurity diffusion in α-Ti was studied most thoroughly in [27]. The authors considered lattice thermal expansion and showed that the difference between the formation energy of substitutional and interstitial impurities decreases with temperature. They also estimated the exponential part of the diffusion coefficient for a number of impurities in both interstitial and vacancy mechanisms, with the difference reaching 9−10 orders of magnitude for Fe and Co. However, direct calculation of the temperature-dependent diffusion coefficient for Fe and other impurities and its comparison with available experimental data [28−30] was not performed. Furthermore, the authors [27] confirmed that the

mechanism involving impurity-vacancy complex formation is not responsible for fast diffusion of several impurities in α-Ti. Thus, currently many phenomena related to impurity diffusion are far from being fully understood even in titanium and its alloys.

The purpose of this work is a theoretical study of iron diffusion in α-Ti within the interstitial and vacancy mechanisms, as well as direct evaluation of the temperature-dependent diffusion coefficient using modern methods.

2. COMPUTATIONAL DETAILS

Calculations of atomic and electronic structure α-Ti were performed using the projector augmented wave (PAW) method [31,32] in a plane-wave basis with the generalized gradient approximation (GGA) [33] for the exchange-correlation functional. A supercell $4 \times 4 \times 3$ containing 96 atoms was used. For atomic structure relaxation, a complete optimization scheme was applied, which allowed changes in both atomic positions and supercell volume. The maximum energy of plane waves from the basis set was 400 eV. Integration over the Brillouin zone was performed using a k-point grid $3 \times 3 \times 3$. Convergence was considered achieved if the difference in total energies between two consecutive iterations did not exceed 10^{-6} eV. Relaxation of atomic positions was carried out until the forces on atoms reached 10^{-4} eV/Å. The calculated lattice parameters were $a = 2.921$ eV and $c = 4.634$ Å and differed from experimental values ($a = 2.951$ Å and $c = 4.684$ Å [34]) by no more than 1%.

The defect formation energy in titanium was calculated using the following formula:

$$E^f = E(\text{Fe} + \text{Ti}) - NE(\text{Ti}) - E(\text{Fe}), \qquad (1)$$

where $E(\text{Fe} + \text{Ti})$ is the total energy of the titanium supercell with an Fe atom, $E(\text{Ti})$ and $E(\text{Fe})$ are the total energies of titanium and iron in their ground states, i.e., Ti in HCP structure and Fe in ferromagnetic BCC structure, parameter N equals 96 in the case of an interstitial defect and 95 when forming a substitutional defect.

Migration barriers were calculated using the climbing image nudged elastic band method CI-NEB [35]. Five images were used to estimate the barriers. The initial position of these images along
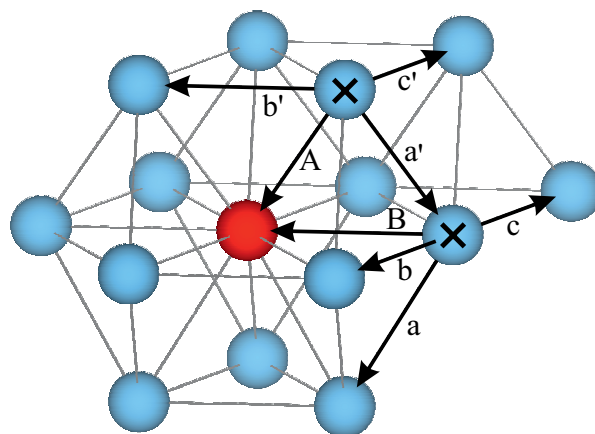
Fig. 1. Schematic representation of atomic jumps within the eight-frequency model. The impurity atom is shown in red, possible initial positions of the vacancy are marked with crosses.

the minimum energy path was found using linear interpolation between the initial and final positions of the diffusing atom. During the relaxation of all five images, each atom was considered elastically bound to the same atom in neighboring images. This approach allows determining the path with the lowest energy, as well as the saddle point. Migration energy barriers of the iron impurity atom were determined as the difference between the total energies of the system at the saddle and initial points.

To estimate the temperature-dependent diffusion coefficient of diffusion within the interstitial mechanism, the Landman method [36, 37] was used, which allows obtaining analytical expressions for this characteristic. Based on the Fourier transform of the displacement matrix $\tilde{p}(\mathbf{k})$ and the Laplace transform of the waiting time density matrix $\tilde{\psi}(u)$, this method assumes to construct a propagator matrix $R(\mathbf{k}, u)$, through which the diffusion coefficient is expressed. A detailed description of this approach is given in our earlier works [38, 39].

To estimate the diffusion coefficient within the vacancy mechanism, as in works [23, 24, 40], the eight-frequency model [41] was used. Within this model, the influence of the impurity is considered only for six jumps, whose initial position is located in the first coordination sphere of the impurity atom, and two more jumps are associated with the exchange of vacancy and impurity positions (Fig. 1). Since two initial configurations of the impurity-vacancy complex are possible, four migration energies need to be calculated for each.
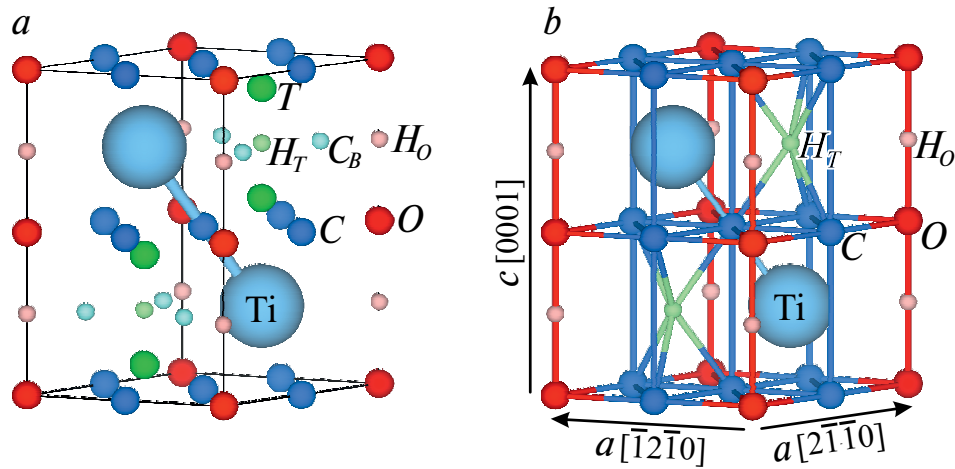
Fig 2. Elementary cell of α-Ti with absorption positions (a), network of possible diffusion paths of Fe atom (b). Large spheres represent titanium atoms, medium red, blue and green spheres represent positions *O*, *C* and *T*, small pink, light blue and light green spheres represent H_O, C_B and H_T

Both methods mentioned above for numerical estimation of the diffusion coefficient require knowledge of jump rates or frequencies, which were calculated using the formula given in [4]:

$$G = \sqrt{\frac{E^m}{2ml^2}} \exp\left(-\frac{E^m + E^f}{k_B T}\right), \quad (2)$$

where E^m is the migration energy of the defect atom, m is the mass of the diffusing atom, l is the jump length, k_B is the Boltzmann constant, T is temperature.

3. RESULTS AND DISCUSSION

3.1. Defect Formation Energies

Titanium in the low-temperature α-phase has a hexagonal close-packed structure with space group No. 194 ($P6_3/mmc$). Titanium atoms occupy 2c-positions according to Wyckoff classification. The following standard interstitial positions were considered as insertion positions (Fig. 2a): octahedral (*O*, in Wyckoff notation positions 2a), tetrahedral (*T*, 4f), two hexahedral positions (H_O, 2b and H_T, 2d) and two crowdions and (*C*, 6_g and C_B, 6h). Note that a crowdion is understood as a position, located on the bond between the nearest matrix atoms. In the case of HCP crystal, there are two crowdion positions: when the impurity atom is located between titanium atoms in the (0001) plane, such position will be denoted as C_B; and when this atom is located between two nearest titanium atoms which are in

adjacent basal planes (*C*-position). Additionally, the substitution position of titanium atom with iron was considered (*S*, 2c). The coordinates of these positions, as well as a number of their structural and energetic characteristics are given in Table 1. During structure optimization with the inserted Fe atom, it turned out that the basal crowdion position (C_B) is not stable, as Fe shifts from it to the *O*-position. Phonon frequency calculations showed that Fe in tetrahedral and both hexahedral positions is characterized by imaginary frequencies, with the latter can be considered as first-order transition states, as Fe has only one imaginary frequency. Thus, in α-Ti for the Fe atom, only positions *O* and *C* will be considered as interstitial positions hereafter, and Fe diffusion can occur through network shown in Fig. 2b.

According to definition (1), a positive value E^f indicates the endothermic nature of defect formation, therefore the lower formation energy corresponds to the more preferable defect. From Table 1, it follows that the crowdion (*C*) is the most preferable interstitial position, and the difference in E_f with *O*-position is 0.26 eV, which satisfactorily agrees with the value of 0.16 eV obtained in work [27], and a slightly lower value of 0.14 eV was obtained in work [26]. To explain the preference of crowdion compared to the octahedral position, mechanical (*MC*) and chemical (*CC*) contributions to the defect formation energy were calculated using the standard procedure, which has been repeatedly applied in earlier works [42,43] for various energy characteristics.

Table 1. Formation energy (*Ef*) of Fe defects in α-Ti(4×4×3), mechanical (*MC*) and chemical (*CC*) contributions, relative change in supercell volume (Δ*V*), bond length d(Fe -Ti), orbital overlap population (θ)

Position	Coordinates	E^f, eV	*MC*, eV	*CC*, eV	Δ*V*, %	d(Fe–Ti), Å	θ(Fe–Ti), el.
O, 2a	(0, 0, 0), (0, 0, 1/2)	1.02, 1.17 [27]	1.47, 1.42 [27]	−0.45, −0.25 [27]	0.75	2.31	0.59
C, 6g	(1/2, 0, 0), (0, 1/2, 0), (1/2, 1/2, 0), (1/2, 0, 1/2), (0, 1/2, 1/2), (1/2, 1/2, 1/2),	0.76, 1.01 [27]	1.63, 1.74 [27]	−0.87, −0.74 [27]	0.74	2.08	0.80
H_O, 2b	(0, 0, 1/4), (0, 0, 3/4)	1.19, 1.38 [27]	1.60, 1.70 [27]	−0.41, −0.33 [27]	0.80	2.10	0.80
H_T, 2d	(1/3, 2/3, 3/4), (2/3, 1/3, 1/4)	2.08	1.82	0.26	0.94	2.22	0.67
T, 4f	(1/3, 2/3, 0.581), (2/3, 1/3, 0.081), (2/3, 1/3, 0.419), (1/3, 2/3, 0.919)	1.35	2.18	−0.83	0.75	1.98, 2.33	0.92, 0.57
S, 2c	(1/3, 2/3, 1/4), (2/3, 1/3, 3/4)	0.59, 0.41 [27]	0.26	0.33	−0.53	in 2.73, out 2.90	in 0.23, out 0.31

It is known that these contributions have opposite signs and their competition determines the preferential positions of incorporation. Although the mechanical contribution in the case of *C*-position exceeds that for *O*-position by 0.16 eV, the chemical contribution in the first case is significantly higher in absolute value by 0.42 eV (0.49 eV [27]). Thus, stronger interatomic interaction Fe–Ti in *C*-position determines its preference compared to *O*-position. When incorporating into the crowdion position, Fe atom causes displacement of nearest Ti atoms by away from it, while the bond length 0.65 Å is 2.08 Å (Table 1). At the same time, Fe incorporation into *O*-position causes significantly smaller displacement of titanium atoms (0.26 Å) and the equilibrium interatomic bond length is considerably larger (2.31 Å) than in the previous case. As shown in Table 1, the supercell volume change for both positions is practically identical (0.74–0.75%). Note that the shorter Fe–Ti bond length also correlates with the higher orbital overlap population value (Table 1), calculated using DDEC6 method [44, 45]. As shown by the calculation of crystal orbital Hamilton population curves (COHP) [46,47], at the Fe–Ti interaction in the considered incorporation positions, no antibonding states are induced (Fig. 3a), which can form in case of impurities with more than half-filled *d*-shell. Note that in *O*-position, the Fe valence band is substantially narrower than in *C*-position, which may indicate relatively weak Fe–Ti interaction in (Fig. 3b).
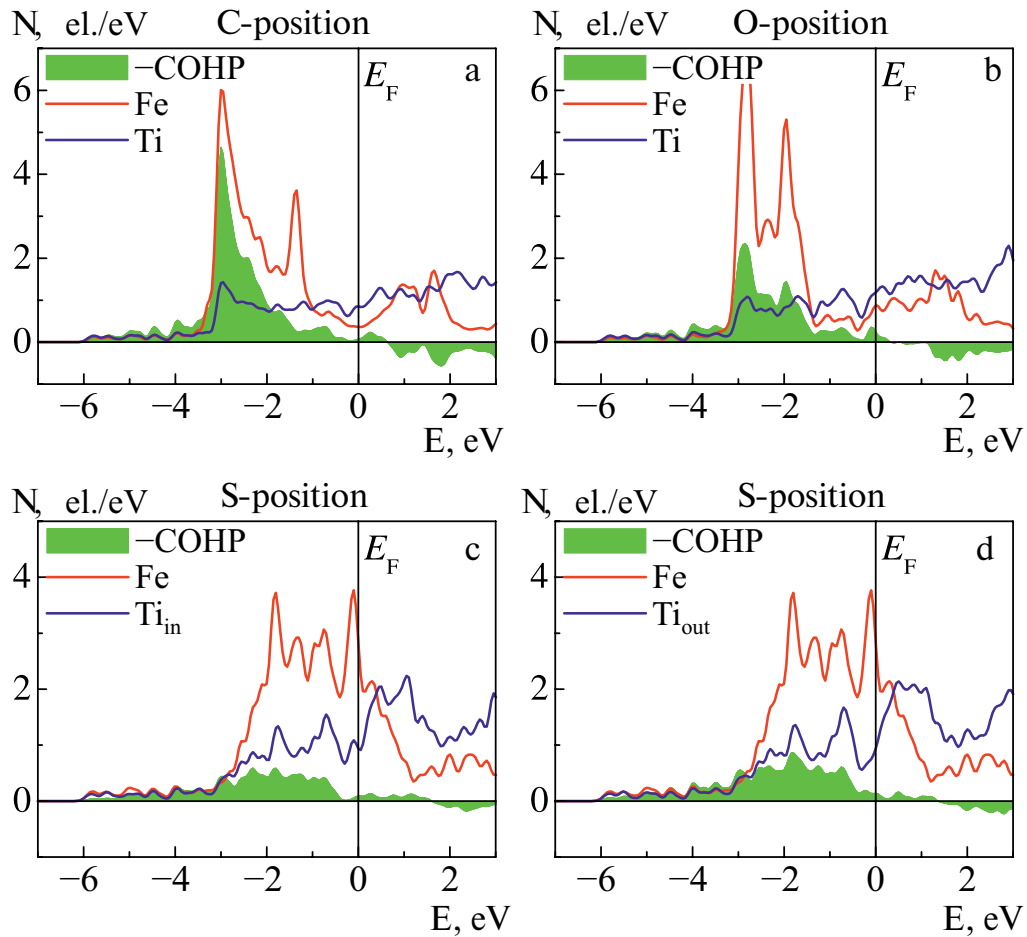
Fig. 3. Local densities of electronic states for Fe atoms (red line) in C- (a), O-(b) and S-position (c, d) and nearest Ti atoms (blue line), as well as COHP curves for Fe−Ti-bonds, shown by filling.

The formation of titanium substitution defect by iron requires only about 0.59 eV, which is 0.17 eV less than the insertion into the crowdion position, while titanium substitution leads to a decrease in the supercell volume (Table 1), as the atomic radius of Fe is smaller than that of the matrix atom. It should be noted that the difference in values E^f of these two defects is significantly lower than the value of 0.60 eV obtained in work [27]. This difference may be related to both different optimization schemes for structures with defects and pseudopotentials. For example, in work [26], where this difference reaches 0.71 eV, the authors used a fixed volume scheme. Information about the used lattice parameters is absent in both works [26,27]. In work [27], the electronic configuration for Fe and Ti included p-electrons, while $3d$- and $4s$-states were considered in present calculations, as in work [26].

Despite the fact that when titanium is substituted by iron, there is a decrease in the length of Fe−Ti_{in} bonds, oriented in the basal plane (0001), by 0.19 Å compared to ideal titanium and, conversely, an increase in the length of bonds between atoms in adjacent planes Fe−Ti_{out} by 0.04 Å, the orbital overlap population of in-bonds remains less than out-bonds. The latter agrees with the lower height of the COHP curve in the case of Ti_{in}, than for Ti_{out} (Fig. 3 c,d). Note that the electronic structure of atoms Ti_{in} and Ti_{ou} differs insignificantly. The energy difference ΔE^f between defects in O- and H_o-positions has a value of 0.17 eV, while values of 0.12 and 0.21 eV were obtained in works [26].

3.2. Interstitial diffusion mechanism

The calculated migration barriers of Fe atom between interstitial positions are shown in Table 2. It can be seen that direct transition between C-positions along the c-axis (Fig. 2b) requires 0.13 eV more energy than in the perpendicular direction. The migration energy of Fe from O-position is small and insignificantly depends on its direction (Table 2). At the same time, the energy

Table 2. Migration energies (E^m in eV) of Fe in α-Ti along two crystallographic directions

Direction	Path	E^m, eV
a	$C \to C$	0.42
	$C \to O$	0.41, 0.33 [27]
	$O \to C$	0.16, 0.17 [27]
c	$O \to (HO) \to O$	0.17, 0.21 [27]
	$C \to (HT) \to C$	1.31
	$C \to C$	0.55

of indirect jump of Fe between crowdions through the saddle H_T-position ($C \to H_T \to C$) along the c-axis is 1.31 eV, which is significantly higher than for direct jump ($C \to C$) along both axes (Table 2). The latter allows excluding this indirect transition from further consideration. Comparison of the calculated energy barriers with available data [27] shows satisfactory agreement.

Since within the Landman method [36, 37] as interstitial positions were used $C(6g)$ and $O(2a)$ and positions, all matrices had the size of 8×8. The obtained expressions for Fe diffusion coefficients along two nonequivalent directions have the following form:

$$D_a = \frac{a^2 G_{OC,a}\left(8G_{CC,a}^2 + 6G_{CC,a}G_{CO,a} + G_{CO,a}^2\right)}{\left(G_{CO,a} + 3G_{OC,a}\right)\left(G_{CO,a} + 3G_{CC,a}\right)} \quad (3)$$

and

$$D_c = \frac{c^2\left(3G_{CC,ñ}G_{OC,a} + G_{CO,a}G_{OO,c}\right)}{4\left(G_{CO,a} + 3G_{OC,a}\right)}, \quad (4)$$

where a, c are lattice parameters, $\Gamma_{ij,k}$ is jump rate $i \to j$ along axis k, which coincides with crystallographic axes.

In Fig. 4, it can be seen that Γ rates differ from each other by several orders of magnitude, particularly $\Gamma_{CO,a}/\Gamma_{OC,a} \approx 0.06$ in the temperature range $500-1150$ K, therefore expressions (3) and (4) can be simplified:

$$D_a = \frac{a^2}{3}\left(G_{CO,a} + 3G_{CC,a}\right) \quad (5)$$

and

$$D_c = \frac{c^2}{4}G_{CC,c} + 0.005c^2 G_{OO,c}. \quad (6)$$

Expressions (5), (6) allow estimating contributions of specific jumps to diffusion coefficients. Approximating the temperature dependence of D_a and D_c according to the Arrhenius equation by least squares method by points with a step of 50 K, we obtain final expressions for diffusion coefficients within the interstitial mechanism:

$$D_a = 4.6 \times 10^{-7}\exp\left(-\frac{1.20}{k_B T}\right) m^2/s,$$
$$D_c = 9.0 \times 10^{-8}\exp\left(-\frac{1.01}{k_B T}\right) m^2/s. \quad (7)$$

In Fig. 5 it is evident that the theoretical values of temperature-dependent diffusion coefficient slightly exceed the experimental values from work [28], where diffusion coefficients were equal to the following expressions:

$$D_a = 6.4 \times 10^{-6}\exp\left(-\frac{1.49}{k_B T}\right) m^2/s,$$
$$D_c = 4.7 \times 10^{-7}\exp\left(-\frac{1.16}{k_B T}\right) m^2/s. \quad (8)$$

Comparing expressions (7) and (8), it is clear that the calculation underestimates the activation energy by approximately $0.15-0.30$ eV, and the pre-exponential factor by $(0.38-5.94) \cdot 10^{-6}$ m^2/ s. In Fig. 5, it is seen, that the anisotropy of Fe diffusion in α-Ti has the correct character ($D_c > D_a$), however, the ratio D_c/D_a is underestimated, although it has the same order. As shown in work [48], calculation of migration barriers using the generalized gradient approximation in PBE form leads to their underestimation by approximately 0.1 eV on average. Additionally, Fe impurity contributes to the weakening of the nearest the Ti−Ti bonds. It can be seen from change in electron localization function (ELF) [49] when titanium is substituted with iron, shown in Fig. 6. The electron localization in the three-center interaction attractor region decreases from 0.8 to 0.6 near the Fe atom, indicating a decrease in covalent and increase in metallic contribution to chemical bonding. The weakening of bonds in α-Ti can also be indirectly seen from the phase diagram of the system Ti−Fe, presented in work [50]. Adding Fe to α-Ti

Table 3. Migration energies calculated within the eight-frequency model

| Jump	A	a'	b'	c'	B	a	b	c
Present results	0.89	0.27	0.10	1.15	0.60	0.07	0.29	0.61
Theory [27]	0.71	–	0.13	–	0.68	0.09	0.30	0.56

reduces the melting temperature, which from the interatomic interaction point of view corresponds to an increase in metallic contribution. When calculating migration barriers, this can lead to overestimated displacements of Ti atoms nearest to Fe, which, in turn, lowers the energy migration barriers. Overall, the order of the ratio of diffusion coefficient to pre-exponential factor at T = 1000 K is 10^{-7}–10^{-6}, while the experimental value equals 10^{-8}–10^{-6} [28]. Note that the difference between theoretical and experimental diffusion coefficient values by one to two orders of magnitude is considered satisfactory, as the experimental results themselves have similar scatter. The approximate estimation of this ratio (10^{-4}) in work [27] is significantly overestimated compared to the experiment.

### 3.3. Vacancy Mechanism of Diffusion

Let's briefly discuss the results obtained for the vacancy mechanism of iron diffusion in titanium. Since the substitution of titanium with iron is the dominant defect, and in [27] only the exponential part of the diffusion coefficient was calculated at a temperature of 1000 K, its estimation within the vacancy mechanism framework is necessary to establish the most preferred mechanism. The obtained migration energy values are shown in Table 3. The vacancy formation energy in pure titanium equals 2.00 eV, which agrees well with the theoretical values of 2.05 eV [27] and 2.08 eV [51], but significantly exceeds the experimental values 1.27–1.55 eV [52,53]. Note that overestimation of vacancy formation energies in metals and alloys is a known issue. Taking into account the temperature contribution to vacancy formation energy allows reducing theoretical values by several tenths of an electron-volt.

Interaction with an iron atom, as mentioned above, weakens Ti-Ti bonding, which leads to a decrease in the formation energy of titanium vacancies. Thus, the formation energy of Ti vacancy in the same atomic layer with orientation (0001), where the iron impurity is located, is 1.62 eV, while vacancy
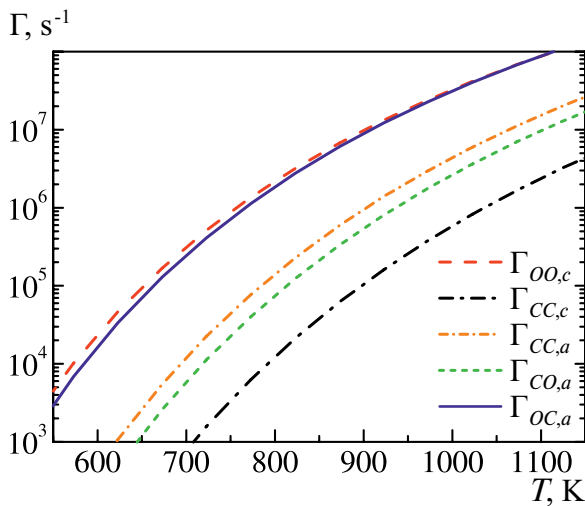
Fig. 4. Temperature dependence of jump rates Γ
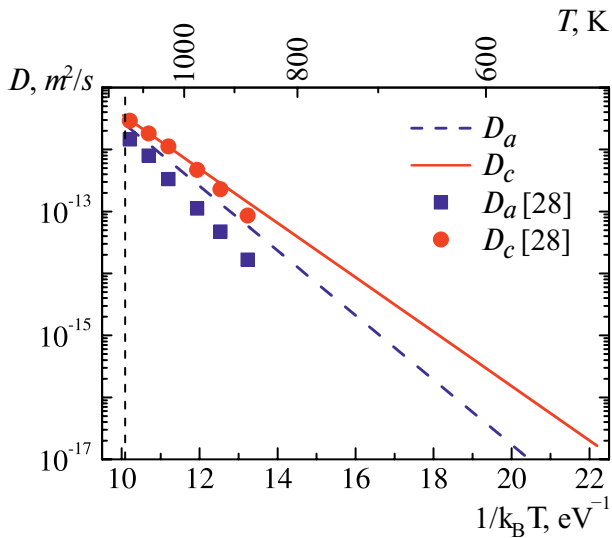
Fig. 5. Temperature-dependent diffusion coefficient of Fe in α-Ti compared with experimental data from [28]. The values obtained in this work are shown by lines, experimental data by symbols. The vertical dashed line corresponds to the phase transition temperature α ↔ β

formation in the adjacent atomic layer near the impurity requires

1.43 eV. Different values suggest that expressions for and should be multiplied by different vacancy concentrations. From an energy point of view, the decrease in vacancy formation energy near the iron impurity is due to the vacancy-impurity interaction energy, which is 0.38 eV and 0.57 eV when both defects are located in the same layer or in adjacent layers, which agrees with the value of 0.50 eV [54] obtained by the Faulkner method.

Within the eight-frequency model, the following expressions were obtained for iron diffusion coefficients along the axes *a* and *c*:

$$D_a = 1.4 \times 10^{-7} \exp\left(-\frac{2.24}{k_B T}\right) m^2 / s,$$

$$D_c = 4.9 \times 10^{-7} \exp\left(-\frac{2.32}{k_B T}\right) m^2 / s. \tag{9}$$

From formulas (9), it follows that the theoretical activation energies in this case significantly exceed the experimental values of 1.16−1.49 eV [28]. The latter indicates that within the vacancy mechanism, high energies are required for elementary jumps between substitution positions. The ratio of the diffusion coefficient to the pre- exponential factor at 1000 K is 10^{-12} (the value 10^{-13} was obtained in work [27]), while within the interstitial mechanism, the value 10^{-7} (in the basal plane) and 10^{-6} (along *c*-axis) was obtained. Thus, despite the fact that the formation of substitution impurity in the case of Fe is more preferable than an interstitial defect, the dominant mechanism is its diffusion through interstitial sites in α-Ti. It should be noted that the temperature effect assessment in [27] on the difference between the formation energies of interstitial and substitution defects showed that it decreases by almost 0.3 eV at 1000 K. In the present work, the difference between these defects at 0 K is only 0.17 eV, and with increasing temperature, the interstitial defect may become dominant. In conclusion, we should also note that in the calculations, the iron concentration was about 1 at.%, while in the experiment it cannot exceed approximately 0.06 at.%. Increasing the number of atoms in the cell leads to significant computational costs and does not affect the obtained migration energy values. Moreover, even in the present model, diffusing atoms do not interact with each other. Therefore, the concentration effect will not affect the values of activation energy and pre-exponential factor.

4. CONCLUSION

The diffusion of iron in α-Ti has been studied using the projector augmented wave method within the interstitial and vacancy mechanisms, and the temperature-dependent diffusion coefficient has been evaluated. The energies of Fe atom incorporation into various interstitial sites were calculated, and it was established that two positions are dynamically stable: octahedral and crowdion. The latter is located between titanium atoms in adjacent basal planes. The formation of a crowdion is energetically preferable (0.76 eV), while the formation of a substitutional defect of titanium with iron requires 0.17 eV less energy, which is consistent with earlier theoretical results. The calculation of iron atom migration energy showed that the lowest barriers correspond to jumps between crowdions in the basal plane (0.41−0.42 eV) and between octahedral positions
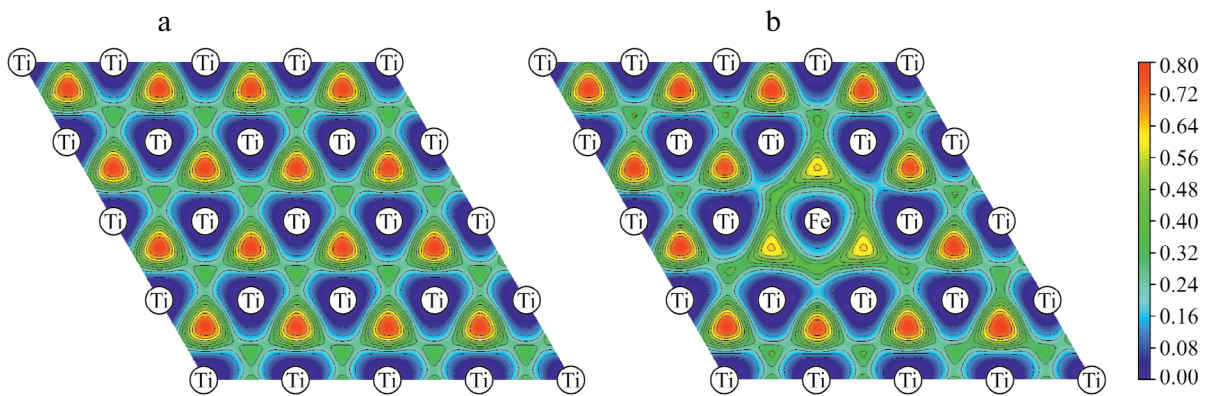
Fig. 6. Electron localization function in pure α-Ti (a) and in the presence of Fe atom (b). The distribution in the (0001) plane is shown. Isolines are drawn in the range from 0 to 0.80 with a step of 0.07

along the *c*-axis (0.55 eV). Analytical expressions for the temperature-dependent diffusion coefficient of iron in α-Ti were obtained within the interstitial mechanism. Numerical evaluation of diffusion coefficients showed that diffusion along the c-axis proceeds faster (activation energy equals 1.01 eV) than in the perpendicular direction (1.20 eV). The theoretical values of the anisotropy parameter D_c/D_a and the diffusion coefficients along two crystallographic directions are in satisfactory agreement with experiment [28], according to which the activation energies are 1.16 and 1.49 eV for diffusion along the *c*-axis and in the perpendicular direction, respectively. At the same time, iron diffusion via the vacancy mechanism requires higher activation energy (2.24−2.32 eV) and proceeds several orders of magnitude slower than interstitial diffusion. Thus, the present research allows us to conclude that for iron in α-Ti, the interstitial diffusion mechanism is preferred.

FUNDING

REFERENCES

1. C. Leyens and M. Peters, Titanium and Titanium Alloys: Fundamentals and Applications, Wiley-VCH Verlag GmbH & Co. KGaA, Weinheim (2003).

2. M. J. Donachie, Jr. Titanium. A Technical Guide (2nd ed.), ASM International, Materials Park, Ohio (2000).

3. M. M. Stupel, M. Bamberger, and M. Ron, J. Less-Common Met. 123, 1 (1986).

4. T. Heumann, Diffusion in Metallen: Grundlagen, Theorie, Vorgänge in Reinmetallen und Legierungen, Springer-Verlag, Berlin (1992).

5. H. Mehrer, Diffusion in Solids: Fundamentals, Methods, Materials, Diffusion-Controlled Processes, Springer, Berlin (2007).

6. Z. Li and W. Gao, in Intermetallics Research Progress, ed. by Y. N. Berdovsky, Nova Sci. Publ., New York (2008), p. 1.

7. D. P. Broom, Hydrogen Storage Materials: The Characterisation of Their Storage Properties, Springer, London (2011).

8. P. Hohenberg and W. Kohn, Phys. Rev. 136, B864 (1964).

9. M. J. Gillan, J. Phys. C: Solid State Phys. 20, 3621 (1987).

10. D. Connétable, Int. J. Hydrogen Energy 44, 32307 (2019).

11. M. G. Shelyapina, Hydrogen 3, 285 (2022).

12. 12. S. E. Kulkova, A. V. Bakulin, and L. S. Chumakova, Phys. Mesomech. 25, 424 (2022).

13. K. Klyukin, M. G. Shelyapina, and D. Fruchart, J. Alloys Compd. 644, 371 (2015).

14. H. H. Wu, P. Wisesa, and D. R. Trinkle, Phys. Rev. B 94, 014307 (2016).

15. A. V. Bakulin, S. S. Kulkov, and S. E. Kulkova, J. Exp. Theor. Phys. 130, 579 (2020).

16. E. Epifano and G. Hug, Comput. Mater. Sci. 174, 109475 (2020).

17. D. Connétable, A. Prillieux, C. Thenot et al., J. Phys.: Condens. Matter 32, 175702 (2020).

18. L. J. Zhang, T. I. Spiridonova, S. E Kulkova et al., Comput. Mater. Sci. 128, 236 (2017).

19. Y. Hu, L. Suo, Q. Long et al., Vacuum 209, 111739 (2023).

20. N. Zou, H.J. Lu, and X.G. Lu, J. Alloys Compd. 803, 684 (2019).

21. G. M. Hood and R. J. Schultz, Philos. Mag. 26, 329 (1972).

22. H. Nakajima and M. Koiwa, ISIJ Int. 31, 757 (1991).

23. L. Scotti and A. Mottura, J. Chem. Phys. 142, 204308 (2015).

24. W. W. Xu, S. L. Shang, B. C. Zhou et al., Phys. Chem. Chem. Phys. 18, 16870 (2016).

25. R. C. Pasianot, R. A. Pérez, V. P. Ramunni et al., J. Nucl. Mater. 392, 100 (2009).

26. R. C. Pasianot and R. A. Pérez, J. Nucl. Mater. 434, 158 (2013).

27. L. J. Zhang, Z. Y. Chen, Q. M. Hu et al., J. Alloys Compd. 740, 156 (2018).

28. H. Nakajima, M. Koiwa, and S. Ono, Scr. Metall. 17, 1431 (1983).

29. H. Nakajima, M. Koiwa, Y. Minonishi et al., Trans. Jpn. Inst. Met. 24, 655 (1983).

30. H. Nakajima and M. Koiwa, in Titanium, Science and Technology, ed. by G. Lütjering, U. Zwicker, and W. Bunk, Deutsche Gesellschaft für Metallkunde e. V., Oberursel (1984), Vol. 3, p. 1759.

31. P. E. Blöchl, Phys. Rev. B 50, 17953 (1994).

32. G. Kresse and D. Joubert, Phys. Rev. B 59, 1758 (1999).

33. J. P. Perdew, K. Burke, and M. Ernzerhof, Phys. Rev. Lett. 77, 3865 (1996).

34. R. M. Wood, Proc. Phys. Soc. 80, 783 (1962).

35. G. Henkelman, B. P. Uberuaga, and H. Jónsson, J. Chem. Phys. 113, 9901 (2000).

36. U. Landman and M. F. Shlesinger, Phys. Rev. B 19, 6207 (1979).

37. U. Landman and M. F. Shlesinger, Phys. Rev. B 19, 6220 (1979).

38. A. V. Bakulin, L. S. Chumakova, and S. E. Kulkova, J. Exp. Theor. Phys. 133, 169 (2021).

39. A. V. Bakulin, L. S. Chumakova, and S. E. Kulkova, Intermetallics 146, 107587 (2022).

40. S. Ganeshan, L. G. Hector Jr., and Z. K. Liu, Acta Mater. 59, 3214 (2011).

41. P. B. Ghate, Phys. Rev. 133, A1167 (1964).

42. A. Y. Lozovoi, A. Alavi, and M. W. Finnis, Phys. Rev. Lett. 85, 610 (2000).

43. S. S. Kulkov, A. V. Bakulin, and S. E. Kulkova, Int. J. Hydrogen Energy 43, 43 (2018).

44. T. A. Manz and N. G. Limas, RSC Adv. 6, 47771 (2016).

45. T. A. Manz, RSC Adv. 7, 45552 (2017).

46. R. Dronskowski and P. E. Blöchl, J. Phys. Chem. 97, 8617 (1993).

47. R. Nelson, C. Ertural, J. George et al., J. Comput. Chem. 41, 1931 (2020).

48. H. Wu, T. Mayeshiba, and D. Morgan, Sci. Data 3, 160054 (2016).

49. B. Silvi and A. Savin, Nature 371, 683 (1994).

50. G. Cacciamani, J. De Keyzer, R. Ferro et al., Intermetallics 14, 1312 (2006).

51. B. Medasani, M. Haranczyk, A. Canning et al., Comput. Mater. Sci. 101, 96 (2015).

52. V. O. Shestopal, Sov. Phys. Solid State 7, 2798 (1966).

53. E. Hashimoto, E. A. Smirnov, and T. Kino, J. Phys. F: Met. Phys. 14, L215 (1984).

54. N. Chen, Z. Yu, Acta Metall. Sin. 30, A112 (1994).